Nanoscale

PAPER

View Article Online
View Journal | View Issue

Cite this: *Nanoscale*, 2025, **17**, 27599

Water-soluble N-heterocyclic carbene stabilized gold nanoparticles by top-down synthesis: performance in catalysis and photoacoustic imaging

Sophie R. Thomas, *[a,b] Ana Luiza de Andrade Querino,[a,c] Guillermo Moreno-Alcántar, [a] Thanh Tran,[a] Tamara Rodríguez-Prieto,[a] Simon Qian, [d] Davide Di Giuseppe,[e,f] Pia Anzenhofer,[f] Vasilis Ntziachristos,[e,f] Heveline Silva,[c] Veronika Somoza, [g,h,i] Roland A. Fischer [j] and Angela Casini *[a]

N-heterocyclic carbenes (NHCs) have emerged as effective capping ligands for gold nanoparticles (AuNPs), offering improved stability and flexibility compared to sulfur-based alternatives. Two synthetic approaches, 'bottom-up' (BU) and 'top-down' (TD), have been described; however, comparative studies remain scarce. Herein, we report the TD-synthesized water-soluble NHC-stabilized AuNPs (NHC@AuNPs) for catalysis in water and biomedical applications, exhibiting exceptional stability in physiologically relevant conditions. Further, the catalytic ability of TD-NPs in model reactions was compared to their BU counterparts featuring the same NHC ligands. In detail, the catalysts were tested for the reduction of 4-nitrophenol and resazurin, as well as for the biomimetic oxidation of 3,3,5,5-tetramethylbenzidine (TMB) in aqueous conditions. The TD-NPs also showed distinct advantages over the BU NPs as contrast agents in photoacoustic imaging (PAI), further highlighting the differences between the two families of colloids.

Received 2nd September 2025,
Accepted 29th October 2025

DOI: 10.1039/d5nr03709c

rsc.li/nanoscale

Introduction

Gold nanoparticles (AuNPs) are amongst the most prominent metal colloids and have become increasingly popular over the last few decades due to their array of applications. Their distinct surface plasmon resonance (SPR), high surface-area-to-volume ratio, and biocompatibility make them benchmark systems in catalysis, materials science, and medicine.[1–4] Over the years, the synthesis of AuNPs has been optimized to precisely control their size and shape, both of which are important for their applications.[5] Another important feature essential for AuNP applicability is colloidal stability; thus, capping ligands are required as stabilizers in solution. Organosulfur-based ligands such as alkyl thiols are the most popular choice due to their high affinity to bind to the 'soft' gold surface.[6] However, the long-term stability of the S–Au bond, especially in physiological conditions, is limited due to the reactivity of thiols to oxidize or be displaced from the NP's surface by competing nucleophiles.

Recently, N-heterocyclic carbenes (NHCs) have emerged as superior AuNP capping ligands.[7] Not only do NHCs offer increased stability due to the strong σ donation of the NHC at the nanoparticle surface, but they are also less prone to oxidative cleavage compared to Au–S. Furthermore, the steric

[a]*Chair of Medicinal and Bioinorganic Chemistry, Department of Chemistry, TUM School of Natural Sciences, Technical University of Munich, 85748 Garching b., Munich, Germany. E-mail: angela.casini@tum.de*
[b]*Department of Inorganic Chemistry, University of Vienna, 1090 Vienna, Austria. E-mail: sophie.rebecca.thomas@univie.ac.at*
[c]*Department of Chemistry, Universidade Federal de Minas Gerais, 31270-901 Belo Horizonte, Brazil*
[d]*Chair of Technical Electrochemistry, Department of Chemistry and Catalysis Research Center, TUM School of Natural Sciences, Technical University of Munich, 85748 Garching b., Munich, Germany*
[e]*Chair of Biological Imaging, Central Institute for Translational Cancer Research (TranslaTUM), School of Medicine and Health & School of Computation, Information and Technology, Technical University of Munich, 81675 Munich, Germany*
[f]*Institute of Biological and Medical Imaging, Bioengineering Centre, Helmholtz Zentrum München, 85764 Neuherberg, Germany*
[g]*Leibniz Institute for Food Systems Biology at the Technical University of Munich, 85354 Freising, Germany*
[h]*Chair of Nutritional Systems Biology, TUM School of Life Sciences, Technical University of Munich, 85354 Freising, Germany*
[i]*Institute of Physiological Chemistry, Faculty of Chemistry, University of Vienna, 1090 Vienna, Austria*
[j]*Chair of Inorganic and Metal-Organic Chemistry, Department of Chemistry, TUM School of Natural Sciences, Technical University of Munich, 85748 Garching b., Munich, Germany*

bulk of the NHC ligand is very different from thiol and phosphine ligands and can influence the association/dissociation behavior and general accessibility of the 'buried' AuNP surface. Overall, NHC ligands provide a versatile scaffold for surface functionalization at the heterocycle backbone and wingtip positions (Fig. 1A), opening new horizons in the applications of these materials in targeted medicine and hierarchical hybrid materials.[8–10] Of note, the carbene platform can also include less classical mesoionic carbenes[11–13] and nitrogen acyclic carbenes.[14]

The two main synthetic routes to form NHC-stabilized AuNPs (NHC@AuNPs) are the 'top-down' (TD)[15] and 'bottom-up' (BU)[16] approaches (Fig. 1B). While the BU strategy involves the direct reduction of preformed Au(I)/(III) NHC complexes, the TD approach is based upon ligand exchange on preformed AuNPs typically capped with alkyl thiol ligands, which are exchanged for the NHC ligands.

The versatility of functionalizing NHCs allows the synthesis of systems bearing water-soluble groups, generating NPs with enhanced colloidal stability in aqueous media. The first examples of water-soluble NHC@AuNPs appeared in 2015, demonstrating the stability of these systems.[17,18] Although there have been a few reports of NHC@AuNP-mediated catalysis in water,[19–22] only one example includes water-soluble NHC@AuNPs.[19]

Furthermore, despite a number of water-soluble NHC@AuNPs being reported over the years,[12,18,23–28] their use in biomedical applications, such as therapy and imaging, or for catalysis in living cells, is still limited.[7] In 2017, Crudden and co-workers reported the ability of small (~3 nm) spherical NHC@AuNPs, bearing carboxylic acid groups on the benzimidazole scaffold, to generate a photoacoustic signal upon irradiation, suggesting these colloids are suitable for photoacoustic imaging (PAI).[23]

In 2019, Johnson and co-workers demonstrated the ability of a bidentate thiolate–NHC–Au(I) complex to be grafted onto the surface of cetyltrimethylammonium bromide (CTAB)-stabilized gold nanorods (NRs) *via* a TD approach.[29] The water-soluble gold nanorods, featuring triazole-conjugated polyethylene glycol, exhibited high stability in biologically relevant conditions and showed promise as photothermal therapeutic (PTT) agents *in vitro*.[29]

Within this framework, Crudden and coworkers reported seminal results highlighting the superiority of 'top-down' synthesized NHC@AuNPs bearing long alkyl chain wingtips.[30] The stability of monodentate and bidentate NHC@AuNPs synthesized by the 'top-down' method was evaluated in tetrahydrofuran (THF) in the presence of dodecanethiol (DDT) and thiophenol, showing superior stability of the bidentate NHC@AuNPs under these conditions.[30]

Furthermore, Reithofer and coworkers recently highlighted the superior stability of water-soluble azide-PEG-NHC@AuNPs formed by the TD *vs.* BU approach in various biomedically relevant conditions.[25]

Despite the rising applications of NHC@AuNPs, and the known influence of the synthesis methodologies on the nanomaterial's properties, there is a lack of systematic studies characterizing the different outcomes of TD *vs.* BU synthetic approaches for the same NHC system in different applications, *i.e.*, catalytic activity.

In 2022, our group studied water-soluble AuNPs with mono- or bidentate NHC capping ligands bearing sulfonate groups on the wingtips, obtained by the BU approach (Fig. 1C).[19] Therefore, in this study, we report the first direct comparison of the catalytic and photoacoustic imaging performance between TD and BU NHC@AuNPs. Thus, first, we report the TD synthesis of AuNPs featuring the same water-soluble sulfonate-bearing NHC ligands of the published BU strategy (Fig. 1C). Then, the obtained NHC@AuNPs were fully characterized by various analytical and spectroscopic measurements, including UV-visible (UV-vis) absorption spectroscopy, NMR spectroscopy, transmission electron microscopy (TEM), dynamic light scattering (DLS), thermogravimetric analysis (TGA), inductively coupled plasma mass spectrometry (ICP-MS), and X-ray photoelectron spectroscopy (XPS). Furthermore, the ability of the TD NPs to catalyze three model reactions in aqueous solution was investigated, and the obtained results were compared to the corresponding BU-made NHC@AuNPs.[19] Firstly, the catalytic reduction of 4-nitrophenol in the presence of sodium borohydride ($NaBH_4$) was used as a model reaction for wastewater remediation and to serve as a benchmark for the catalytic ability of AuNPs. Next, the reduction of resazurin forming fluorescent resorufin in the presence of hydroxylamine (NH_2OH) was considered, providing a model reaction for a NP-catalyzed bioorthogonal transformation in aqueous solution.[31] Additionally, the NPs were

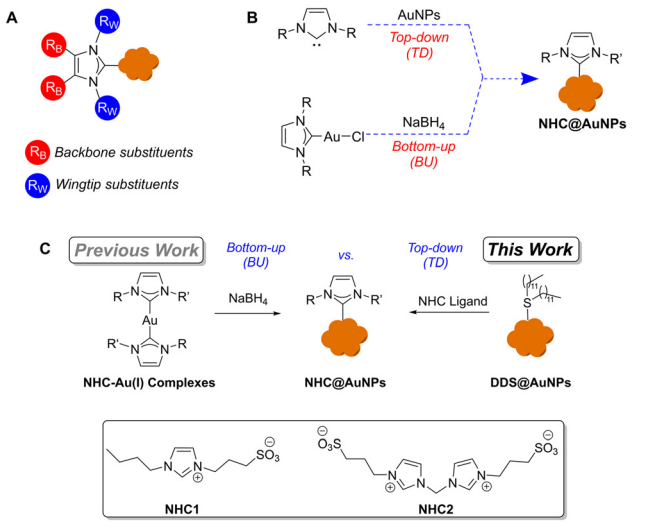

Fig. 1 A. NHC@AuNP structure with possible sites for functionalization highlighted (backbone and wingtips). B. General synthesis scheme to produce NHC@AuNPs *via* either the 'top-down' or 'bottom-up' approach ($NaBH_4$ = sodium borohydride). C. Synthesis of water-soluble NHC@AuNPs by the 'bottom-up' approach (previous work) and by the 'top-down' approach (this work). Exert shows the selected hydrophilic sulfonate imidazolium salts as NHC precursors.

tested as peroxidase mimics using the colorimetric 3,3,5,5-tetramethylbenzidine (TMB) oxidation reaction in the presence of hydrogen peroxide (H_2O_2) as an alternative to the enzyme horseradish peroxidase (HRP), which is commonly used in biosensing applications.[32] Due to the elevated cost and low environmental stability of HRP, enzyme-mimicking NPs for biosensor development have become more popular over the years.[32,33] Finally, we studied the preliminary PAI performance of the NHC@AuNPs as contrast agents produced by either the TD or the BU synthesis using multispectral optoacoustic tomography (MSOT).[34] Altogether, our results demonstrate that the physicochemical, catalytic, and photoacoustic properties of NHC@AuNPs are significantly influenced by the selected synthetic strategy, highlighting the need for a mindful choice of approach when designing NHC@AuNPs for different applications.

Results and discussion

The soluble sulfonated N-heterocyclic imidazolium salts, **NHC1** and **NHC2** (Fig. 1C), and the corresponding BU nanoparticles (**AuNP1-BU** and **AuNP2-BU**, respectively) were synthesized according to previously reported methods.[19,35,36] To obtain the TD NPs, dodecyl sulfide (DDS)-stabilized gold nanoparticles (**DDS@AuNPs**) were prepared following the Brust-Schiffrin method.[37] Afterwards, the water-soluble TD-NHC@AuNPs were synthesized by the *in situ* deprotonation of the imidazolium salts (**NHC1** and **NHC2**) with potassium *tert*-butoxide before the addition of **DDS@AuNPs**, yielding the NHC-stabilized **AuNP1-TD** and **AuNP2-TD**, respectively (Fig. 1C). The resulting NPs were then isolated by centrifugation and purified by extensive dialysis and lyophilization before characterization (see Experimental for details).

After ligand exchange, the synthesized TD-NHC@AuNPs' SPR band was slightly blue-shifted compared to the precursor **DDS@AuNPs** (**DDS@AuNPs** = 520 nm, **AuNP1-TD** = 512 nm, **AuNP2-TD** = 514 nm, Fig. S1). Further, the displacement of DDS by the NHC ligand on the surface of the NPs after dialysis was confirmed by ^{1}H NMR spectroscopy (Fig. S2 and S3) with no evidence of DDS present in the purified material when compared to the ^{1}H NMR of **DDS@AuNPs** in the literature.[17] The disappearance of the H_a imidazolium proton resonance, a slight shielding of the imidazole protons, and general broadening of the signals[38,39] for both **AuNP1-TD** and **AuNP2-TD** confirms the formation of the carbene species and completion of the metalation reaction *via* coordination to Au(0), meaning no free NHC ligand was available on the NP surface. Both ligands, **NHC1** and **NHC2**, show diastereotopic peaks upon coordination to the AuNPs due to the restricted bond rotation.

By TEM, the TD NHC@AuNPs appear *quasi*-spherical, with a narrow size distribution and a similar size to that of the precursor **DDS@AuNPs** (5.7 ± 0.9 nm, 4.9 ± 0.9 nm, and 4.7 ± 1.6 nm for **DDS@AuNPs**, **AuNP1-TD,** and **AuNP2-TD**, respectively, Fig. S4 and Fig. 2A, B; Table 1). Additionally, no significant aggregation or etching of the NPs is observed after ligand exchange.

Furthermore, DLS in MilliQ H_2O shows hydrodynamic sizes of 13 ± 3 nm for **AuNP1-TD** (Fig. 2C and Table 1) and 18 ± 5 nm for **AuNP2-TD** (Fig. 2D and Table 1); the difference in size can be explained by the highly charged hydrophilic surface of the NPs creating a solvation/counterion shell of ~8 nm for **AuNP1-TD** and ~13 nm for the more densely charged **AuNP2-TD**. The low PDI values highlight the homogeneity of the samples.

Indeed, ζ-potential measurements were also performed to understand the electrostatic interactions between the particles, which can indicate charge-induced stability of the colloidal dispersions in aqueous solution.[40]

The TD NHC@AuNPs exhibited ζ-potentials around −20 mV, while the BU NHC@AuNPs showed values ranging from −25 mV to −38 mV, all consistent with the presence of negatively charged sulfonated groups (Fig. 2E). This suggests that the layer of electrostatic stabilization is slightly higher for BU-AuNPs compared to the TD-AuNPs, with values above 30 mV or below −30 mV considered the most stabilizing.[41]

The thermal stability of the NHC@AuNPs was evaluated by TGA (Fig. 2F), with markedly lower desorption temperatures of ligand loss observed for the precursor **DDS@AuNPs** (~210 °C, Fig. 2F) compared to the NHC@AuNPs (**AuNP1-TD** = ~400 °C and **AuNP2-TD** = ~420 °C, Fig. 2F) supporting the successful occurrence of complete ligand exchange based on the increased stability of the NHC ligands on the AuNP compared to thiol alternatives. The BU NPs also showed similar desorption temperatures for ligand loss.[19] Furthermore, ICP-MS studies (Table 1) were conducted to assess the overall gold content, which is relevant for further catalysis studies.

Additionally, XPS was used to confirm the surface composition of the NPs, including the Au(0)/Au(I) ratio. The TD approach yielded NPs with Au(0) content >96% (Fig. 2G), which is significantly higher compared to the BU NHC@AuNPs, whereby a substantial percentage of Au(I) was retained.[19] The presence of characteristic C 1s peaks corresponding to C–C and C–N could also be observed using XPS in both **AuNP1-TD** and **AuNP2-TD** at *ca*. 285 and 286 eV, respectively (Fig. S5A and B, Table S1), as well as the N 1s peak *ca*. 401 eV (Fig. S6A and B, Table S1). Furthermore, the ligand : Au ratio on the NP surface can be estimated by XPS due to the presence of sulfur on both of the NHC ligands, assuming quantitative replacement of the DDS ligand with the NHC ligand. This assumption is valid since no traces of DDS ligand are present in the corresponding ^{1}H NMR spectra of the purified AuNPs (Fig. S2 and S3). Using the S 2p peak, we can calculate for **AuNP1-TD**, the L : Au ratio to be 0.27, and for **AuNP2-TD**, the L : Au ratio to be 1.16 (taking into account the presence of one and two sulfoxide groups in **NHC1** and **NHC2**, respectively, using relative sensitivity factors of 6.25 for Au 4f and 0.668 for S 2p),[42,43] highlighting the higher ligand coverage of **NHC2** on the AuNP surface.

The colloidal stability of the TD NHC@AuNPs was further demonstrated over time (16 h) in MilliQ water at 37 °C by UV-

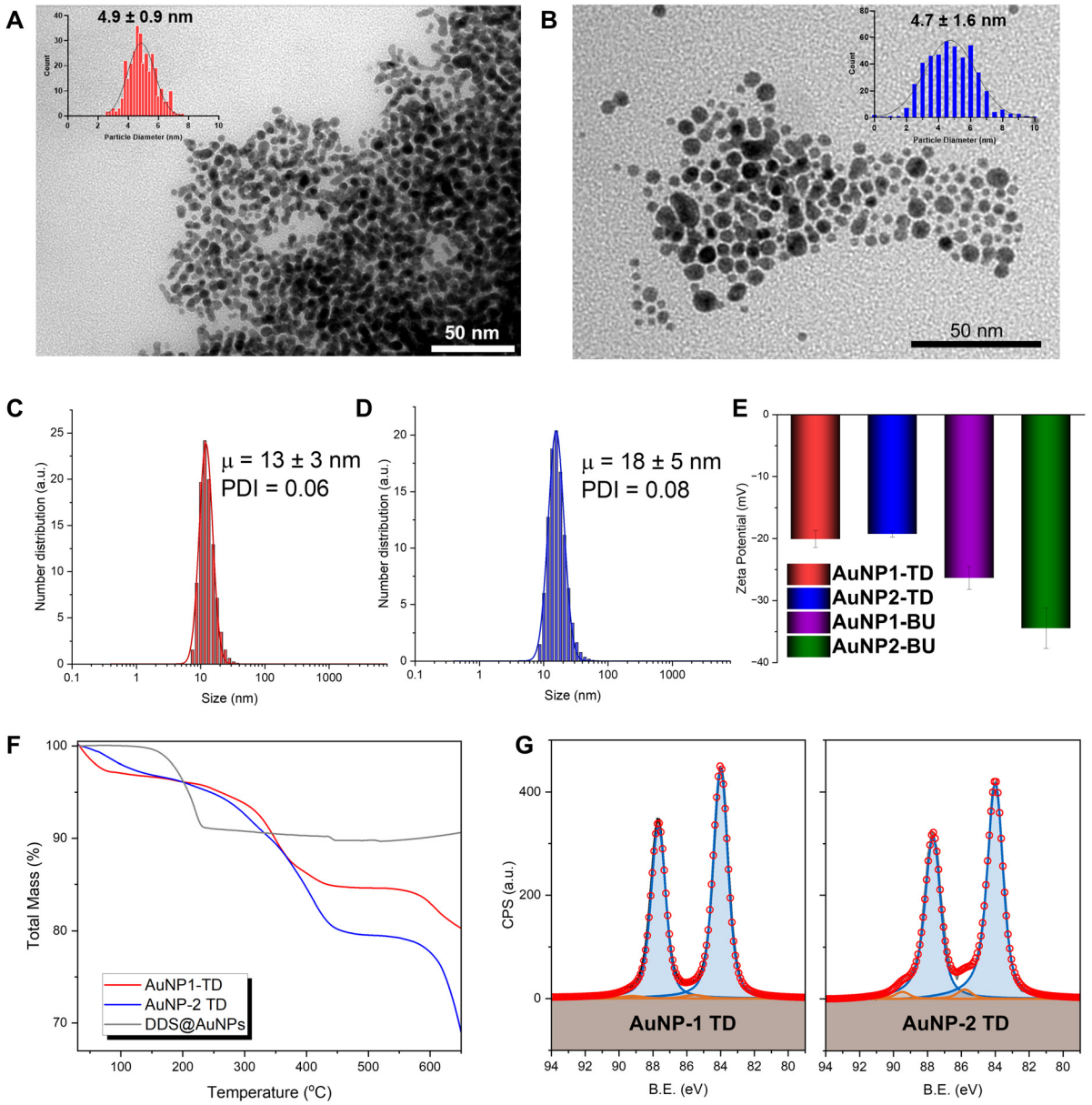

Fig. 2 TEM representative image of the A. **AuNP1-TD** and B. **AuNP2-TD** with size histogram and average particle size. Average DLS traces of C. **AuNP1-TD** and D. **AuNP2-TD** in MilliQ water over three measurements. E. Average zeta potentials (mV) of the two families of NHC@AuNPs with standard deviation over three measurements. F. TG graphs of **AuNP1-TD** (red line), **AuNP2-TD** (blue line), and **DDS@AuNPs** (grey line) under a controlled atmosphere. G. XPS spectra of the Au 4f region in **AuNP1-TD** and **AuNP2-TD** (Au(I) in orange and Au(0) in blue). Au(0) area was used for spectra normalization, while the normalized spectra are shown after Shirley background subtraction to provide a comparison.

Table 1 Properties of the investigated TD NHC@AuNPs in this work and previously investigated BU NHC@AuNPs

NHC@AuNPs	Au particle size[a] [nm]	Hydrodynamic size[b] [nm]	Au wt[c] [%]	Au(0) content[d] [%]	Zeta potential[e] (mV)
DDS@AuNPs	5.7 ± 0.9	n.d.	n.d.	n.d.	n.d.
AuNP1-TD	4.9 ± 0.9	13 ± 3	10.9	98	−20.1 ± 1.4
AuNP2-TD	4.7 ± 1.6	18 ± 5	38.3	96	−19.3 ± 0.5
AuNP1-BU	2.3 ± 1.1[f]	n.d.	12.6[f]	72[f]	−26.4 ± 1.9
AuNP2-BU	2.6 ± 1.2[f]	n.d.	29.0[f]	38[f]	−34.5 ± 3.3

n.d. = not determined. [a] Average diameter of the AuNPs and standard deviation values as determined by TEM analysis. [b] Average hydrodynamic size of the AuNPs in MilliQ H_2O and standard deviation values over three measurements determined by DLS analysis. [c] Au weight percentage determined by ICP-MS. [d] Au(0) content percentage estimated by XPS analysis. [e] Zeta potential measurement obtained as an average over three experiments with standard deviation. [f] From ref. 19.

visible absorption spectroscopy (Fig. S7A and B). Both TD-NPs exhibited high stability with no significant changes to the SPR bands over time. Similar results were observed in PBS 1× (phosphate buffered solution, pH 7.4) in the presence of serum albumin (bovine serum albumin, BSA 17 mM) (Fig. S8A and B), the most abundant protein in the mammalian bloodstream.[44] In this more complex solution, the high stability of the TD NHC@AuNPs remained, with negligible variations in the SPR band over 16 h, which was consistent with the results obtained for the BU NHC@AuNPs.[19] In contrast, thiol-stabilized AuNPs, such as **DDS@AuNPs**, suffer low stability in these conditions (data not shown).[45]

It should also be noted that the TD NHC@AuNPs showed no cytotoxicity in HGT-1 cells over 24 h (IC_{50} = <100 μg mL^{-1}, data not shown), which is similar to the results observed for the BU NHC@AuNPs in PC-3 cells over 24 h.[19]

Overall, the TD and BU AuNPs present important differences in chemical and structural factors that typically play a role in the catalytic efficiency of gold nanoparticles. For example, a higher concentration of Au(0) may provide more active sites for catalysis, potentially leading to enhanced reaction rates. However, this varies depending on the reaction studied. Similarly, the size of NPs is another crucial factor. Smaller NPs generally possess a higher surface-area-to-volume ratio, offering more catalytically active sites per unit mass than larger NPs.[46] Additionally, the amount of ligand coverage must be carefully balanced: without stabilizing ligands, the NPs will suffer from aggregation. However, the ligand shell lowers the activity since there is reduced surface accessibility.[47] Therefore, since the TD and BU NHC@AuNPs display differences in the features described above, we evaluated the catalytic ability of the different NPs in three benchmark reactions, namely the reductions of 4-nitrophenol and resazurin and the peroxidase-mimicking oxidation of 3,3,5,5-tetramethylbenzidine (TMB), all of which are performed in an aqueous environment.

The TD NHC@AuNPs were first tested against the reduction of 4-nitrophenol with $NaBH_4$ in water, a model reaction used for wastewater remediation.[19] In detail, the formation of 4-aminophenol (λ_{max} = 300 nm) was monitored by UV-vis absorption spectroscopy over time, following the decrease in the concentration of 4-nitrophenolate at 400 nm (see exemplary spectrum in Fig. S9A). The catalytic reduction of 4-nitrophenol was performed with 0.2 mg of **AuNP1-TD** (Au = 10.9 μg mL^{-1}) and 0.3 mg of **AuNP2-TD** (Au = 57.45 μg mL^{-1}), respectively, under the same conditions as the previously reported BU-formed NPs.[19] To correct for the difference in NP mass, the rate constants (k) were normalized (k_{nor} = k/mass), as previously described by Ribot and coworkers.[11] In this reaction, **AuNP1-TD** displays a higher k of 0.74 ± 0.11 min^{-1} (k_{nor} = 3.7 min^{-1} mg^{-1}), with respect to **AuNP2-TD** (k = 0.39 ± 0.010 min^{-1}, k_{nor} = 1.4 min^{-1} mg^{-1}) (Fig. S9B). This can be explained by the nature of the bidentate ligand **NHC2**, which could result in more hindered access of the substrate to the binding sites on the NP surface due to a thicker ligand shell, despite the higher Au(0) content on the surface of these AuNPs. This trend was also observed for the BU NPs[19] with k = 1.4 min^{-1} (k_{nor} = 7 min^{-1} mg^{-1}) and 0.21 min^{-1} (k_{nor} = 0.7 min^{-1} mg^{-1}), for **AuNP1-BU** and **AuNP2-BU**, respectively.

Moreover, when comparing the **AuNP1-TD** to the corresponding **AuNP1-BU**, the rate constant of the latter appears nearly 2-fold higher than that of the TD NPs (k_{nor} = 3.7 min^{-1} mg^{-1} *vs.* 7 min^{-1} mg^{-1} for **AuNP1-TD** and **AuNP1-BU**, respectively).[19] Taking into account the similar gold content of both systems ([Au] = 10.9 μg mL^{-1} and 12.6 μg mL^{-1}, respectively), the difference in catalytic activity can be explained by the favorable smaller size of the BU NPs (Table 1), which increases their surface-area-to-volume ratio, and the number of catalytically active sites. On the contrary, in the case of larger **AuNP2-TD**, the rate constant is almost double that of **AuNP2-BU** (k_{nor} = 1.4 min^{-1} mg^{-1} *vs.* 0.7 min^{-1} mg^{-1}, respectively). This can be due to the significantly higher percentage of Au(0) on the surface of the TD NPs (Table 1) and the slightly higher Au content (Au = 57.45 μg mL^{-1} and 43.5 μg mL^{-1} for **AuNP2-TD** and **AuNP2-BU**, respectively), which together outweighs their larger size.[19]

Additionally, the catalytic activity of the NPs was also assessed for the reduction of resazurin with NH_2OH in water, a biocompatible model reaction that is used to assess cell viability.[48] This reaction can be monitored by fluorescence spectroscopy due to the formation of the fluorescent product resorufin at 584 nm over time. Since an excess of NH_2OH is used, the rate constant (k) of the reaction can be determined by assuming a *pseudo*-first-order reaction.[49] To assess the rate constant for resazurin reduction, kinetic fluorescent studies were carried out in a plate reader with low concentrations of the NPs (1.8 μg mL^{-1}) and resazurin (4.5 μM) to avoid inner filter effects. Since all NP solutions have the same concentration in each well (1.8 μg mL^{-1}), the rate constants can be compared directly. In the case of **AuNP2-BU**, no catalytic activity was observed at these concentrations, which could be related to the lower Au(0) surface content. Instead, **AuNP2-TD** showed the highest rate constant (k = 3.7 × 10^{-3} ± 6 × 10^{-5} min^{-1}, k_{nor} = 0.02 min^{-1} μg^{-1}) compared to **AuNP1-TD** (k = 7.0 × 10^{-4} ± 1 × 10^{-5} min^{-1}, k_{nor} = 0.004 min^{-1} μg^{-1}) and **AuNP1-BU** (k = 6.0 × 10^{-4} ± 1 × 10^{-5} min^{-1}, k_{nor} = 0.003 min^{-1} μg^{-1}) (Fig. S10).

Metal NPs are among the more promising artificial peroxidases, with AuNPs already proposed as effective peroxidase-mimicking catalysts;[50–53] however, to date, no NHC@AuNPs have been used for this purpose, and only one example uses a NHC-stabilized heterometallic system (NHC@AuPdNPs).[54] The generation of peroxidase-like active artificial systems, able to operate in conditions other than those of biological relevance, has big potential in chemical synthesis, wastewater remediation, biotechnology, and sensing, among other applications.[55] Peroxidases are a group of enzymes that allow hydrogen peroxide-mediated oxidations into water and free radicals.[55] To assess the catalytic activity of our NPs, we followed the oxidation of TMB in the presence of H_2O_2, profiting from the production of a charge transfer complex with distinctive absorptions at 370 and 650 nm,[56] which were monitored *via* UV-vis

absorption spectroscopy (Fig. 3). The reaction was performed at pH 4 and 37 °C, over 25 min for the different NHC@AuNPs obtained *via* TD or BU approaches. To compare the different NPs, the turnover frequency (TOF) values for the oxidation of TMB were calculated using the initial rates approximation (see SI); the TOF values referred to the total amount of gold as measured by ICP-MS (Table 1).

The results obtained show that both TD and BU NPs are able to catalyze this reaction. Interestingly, AuNP2 exhibits markedly faster conversion compared to AuNP1 for both synthetic methods (Fig. 3A). This can be due to an increased negative charge density when the **NHC2** ligand is used, which will electrostatically interact with the positively charged TMB molecule, protonated at the reaction conditions.[57–59] However, while this explanation is corroborated by the more negative ζ-potential of **AuNP2-BU** compared with **AuNP1-BU**, the TD NPs display very similar ζ-potentials, suggesting different effects also play a role in this reaction.

When comparing the different synthetic approaches, the BU NHC@AuNPs show consistently lower TOF per mol of gold (mol_{TMB} mol_{Au}^{-1} s^{-1}) regardless of the ligand used when compared to the TD counterparts (Fig. 3B, purple bars). Accordingly, the molecular Au(I) NHC compounds **AuNHC1** and **AuNHC2** did not show any catalytic activity (Fig. S11).

Finally, we carried out phantom studies to investigate the potential of these water-soluble NHC@AuNPs as contrast agents for photoacoustic imaging (PAI), which is a noninvasive imaging technique often used for the diagnosis of disease.[60] Thus, we tested the TD and BU NHC@AuNPs obtained with the **NHC2** ligand (**AuNP2-TD** and **AuNP2-BU**) in a tissue phantom model using wavelengths within the 'biological window', where less blood and tissue attenuation are expected.[61] We compared the performance of **AuNP2** synthesized by BU and TD approaches to evaluate the influence of the Au(0) surface content and NP size on their performance (Table 1). Three different concentrations of the NPs were measured using the multispectral optoacoustic tomography (MSOT, Fig. S12) device within a tissue phantom. MSOT is an advanced optoacoustic approach whereby tissues can be imaged at multiple wavelengths rather than a single excitation wavelength and then processed by unmixing algorithms. This allows the intrinsic chromophores, such as hemoglobin and melanin, to be distinguished, as well as any exogenous agents used,[62] such as AuNPs.

First, the photoacoustic spectra of the samples were measured between 660–980 nm by calculating the average photoacoustic response in a cross-sectional area of 5 mm^2 located inside the sample straw. Both synthesis approaches exhibit a consistent linear decline in response to the wavelength increases, with a pronounced dip occurring at 950 nm (Fig. S13A and B). To assess the relative photoacoustic amplitude in relation to NP concentration, we focused on three distinct wavelengths: 675 nm, commonly utilized for melanin sensing; 805 nm, representing the oxy-deoxy isosbestic point; and 930 nm, chosen for its relevance to lipids.[60] Specifically, **AuNP2-TD** demonstrated a notably stronger PA response and more linear relationship (R^2 > 0.99) with increasing concentrations, as illustrated in Fig. S14A. Conversely, the **AuNP2-BU** showed a non-linear effect for the higher concentrations (Fig. S14B). The concentration and 3D distribution of nanoparticles throughout the entire measured volume were then visualized using MSOT. The results revealed that the TD NPs (Fig. 4A) exhibit exceptionally higher photoacoustic contrast

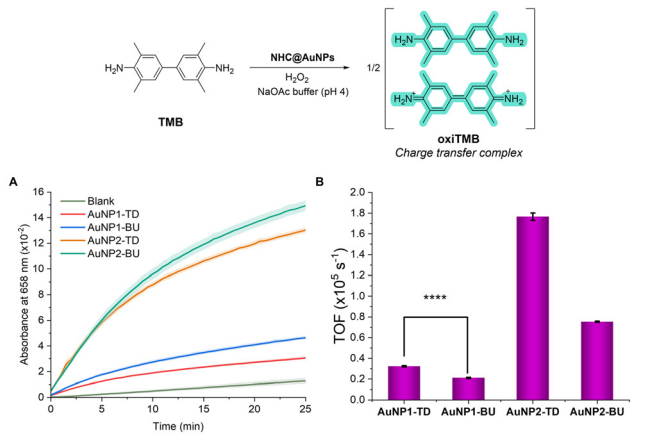

Fig. 3 A. UV-vis absorption kinetics (658 nm) for the oxidation of TMB with NHC@AuNPs in the presence of H_2O_2 over 25 min at 37 °C in NaOAc buffer (pH 4.0). Kinetics of reaction shown without catalyst (blank, green line, two experiments), with the addition of **AuNP1-TD** (red line, Au = 0.05 μg mL^{-1}), **AuNP1-BU** (blue line, Au = 0.12 μg mL^{-1}), **AuNP2-TD** (orange line, Au = 0.05 μg mL^{-1}) and **AuNP2-BU** (teal line, Au = 0.12 μg mL^{-1}) with lines corresponding to an average of three experiments with standard deviation represented by splice. B. TOF values for NHC@AuNPs based on μg of Au (purple bars) in the sample. Statistical significance by nonparametric *t*-test (*$P \leq 0.05$, ****$P = 0.00006$).

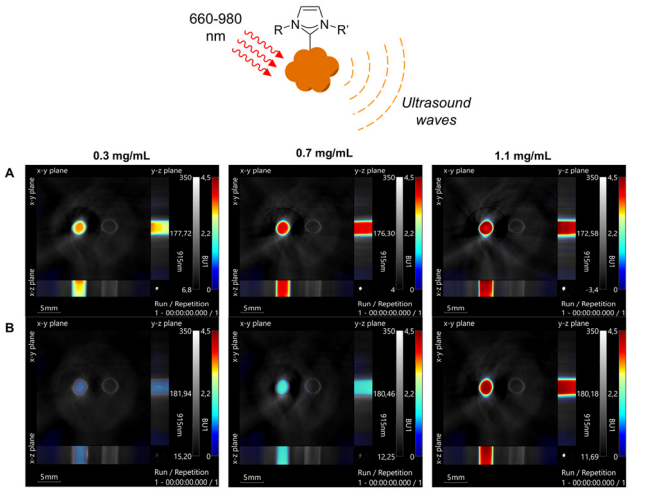

Fig. 4 Cartoon representation of the photoacoustic imaging (PAI) effect. Optoacoustic images showing the orthogonal views of the measured phantoms when irradiated with 65 different wavelengths ranging from 660 to 980 nm. The color intensity represents an unmixed spectrum for the respective NHC@AuNP concentrations. The grayscale background corresponds to the total PA response at 915 nm. A. **AuNP2-TD** and B. **AuNP2-BU**.

compared to the BU NPs (Fig. 4B), with a uniform response even within the 'biological window' despite the location of the SPR band at *ca.* 500 nm, far from 660–980 nm. The difference between the two samples is particularly evident at the lower concentrations. Furthermore, since the NPs cannot resonate with the NIR irradiation directly, this effect can be due to two-photon absorption, which we previously observed for the photothermal effect of the BU NHC@AuNPs.[19]

Due to the photoacoustic amplitude being an arbitrary value that is dependent on many factors within the setup, it is difficult to directly compare the response to existing data. Usually, larger AuNPs and gold nanorods are used for these studies due to their NIR SPR bands.[63–65] For example, AuNRs at a concentration of 0.08 mg mL^{-1} showed a PA signal of *ca.* 250 a.u. in a similar phantom setup.[66] Furthermore, biodegradable gold vesicles formed from an assembly of AuNPs exhibited a significantly higher photoacoustic response (approximately 10-fold) compared to AuNRs, both with an optical density of 1.0.[67] However, studies with small nanoparticles are scarce, and no data has been previously reported on applying NHC-stabilized AuNPs within this setup. Overall, the results obtained in this tissue-mimicking phantom are encouraging and suggest further applicability that should be studied *in vivo* to assess clinical translation.

Conclusions

Here, we have successfully synthesized two different water-soluble NHC@AuNPs by the 'top-down' (TD) approach and compared their properties to 'bottom-up' (BU) NHC@AuNPs, featuring the same hydrophilic NHC ligands.[19] Various methods were used to fully characterize the NPs, demonstrating the successful ligand exchange between the DDS and NHC ligands on the NP surface. In addition, the NPs formed by the TD approach were slightly larger (~5 nm) than the BU NPs (~2 nm) due to retention of the precursor **DDS@AuNPs** size, with a significantly higher percentage of Au(0) (>96%). Importantly, the high stability in physiologically relevant solutions was retained, as observed for the BU NPs.[19]

Moreover, the catalytic ability of the TD NPs was demonstrated for the reduction of 4-nitrophenol and compared to the corresponding BU NPs. Within the general trend, it is worth noting that the larger size of the **AuNP1-TD** resulted in a lower catalytic activity compared to the smaller **AuNP1-BU**, despite the markedly increased Au(0) content. In the case of the resazurin reduction, **AuNP2-TD** showed the highest rate constant, with **AuNP1-TD** and -BU performing similarly. **AuNP2-BU** showed no activity at these concentrations, following a similar trend as observed for the 4-nitrophenol reduction.

Additionally, the NPs were identified as peroxidase mimics by catalyzing the decomposition of hydrogen peroxide in the presence of TMB, which can result in more stable and cheaper alternatives to horseradish peroxidase[55] for applications such as DNA sensing. Interestingly, AuNP2 colloids synthesized by both methods outperformed the respective AuNP1, which we postulate may be due to the increased negative charge localization on the NHC ligands, offering electrostatic attraction to the TMB molecule.

Finally, in preliminary studies, the NPs were investigated as photoacoustic imaging (PAI) probes using multispectral optoacoustic tomography (MSOT) within a tissue-mimicking phantom. Despite their small size compared to classical nanorod systems, the investigated **AuNP2-TD** showed a high photoacoustic signal that increased linearly with concentration despite the use of wavelengths within the biological window. Overall, our work highlights that besides the generally desirable properties of NHC@AuNPs for catalysis and medicinal applications, significant differences emerge when different synthetic routes are applied to generate otherwise closely related materials, calling for attention to tailoring the synthetic method to the desired application. These cautions must be applied in future work involving the bioconjugation of targeting molecules to the NHC ligand, such as peptides, which could be used for targeted PAI and PTT. This could also be combined with catalysis in cells for the activation of a prodrug or uncaging of a fluorophore, providing a novel multimodal platform for disease diagnosis and management.

Author contributions

S. R. T. and A. C. were responsible for the project conceptualization and supervision. S. R. T. and A. L. A. Q. wrote the first draft of the manuscript, and all co-authors contributed to the results and discussion sections. S. R. T., A. L. A. Q., G. M.-A., and A. C. designed the graphics. S. R. T., A. L. A. Q., and T. T. performed the synthesis and characterization of the AuNPs. G. M.-A. performed the catalysis reactions and evaluated the data. T. R.-P performed the ICP-MS experiments with expertise and resources from V. S. S. Q. carried out XPS experiments and data analysis. D. D. G., P. A., and V. N. contributed to and supervised the photoacoustic measurements. H. S. provided expertise on synthesis. R. A. F. provided expertise on material characterization.

Conflicts of interest

V. N. is a founder and equity owner of Maurus OY, sThesis GmbH, Spear UG, Biosense Innovations P.C. and I3 Inc. All other authors declare that they have no competing interests.

Data availability

The authors confirm that the data supporting this article is available within the article and the supplementary information (SI). Supplementary figures, materials, and methods are included in the SI. See DOI: https://doi.org/10.1039/d5nr03709c.

Acknowledgements

S. R. T. acknowledges the TUM Global Postdoc Fellowship Scheme for funding and the FWF (Austrian Science Fund) for the ESPRIT fellowship (10.55776/ESP708). A. L. A. Q. acknowledges the funding from Coordenação de Aperfeiçoamento de Pessoal de Nível Superior – Brasil (CAPES, Finance Code 001). T. R. P. acknowledges Margarita Salas research grant from the Ministry of Universities of Spain for funding. Dr Carsten Peters (TUM) is kindly acknowledged for his assistance recording TEM data. S. Q. gratefully acknowledges funding by the Deutsche Forschungs-Gemeinschaft (DFG, German Research Foundation) under Germany's Excellence Strategy-EXC 2089/1-390776260. H. S. thanks CNPq (314399/2023-2) for research fellow.

References

1 M. C. Daniel and D. Astruc, Gold Nanoparticles: Assembly, Supramolecular Chemistry, Quantum-Size Related Properties and Applications toward Biology, Catalysis and Nanotechnology, *Chem. Rev.*, 2004, **104**, 293–346.
2 K. Saha, S. S. Agasti, C. Kim, X. Li and V. M. Rotello, Gold nanoparticles in chemical and biological sensing, *Chem. Rev.*, 2012, **112**, 2739–2779.
3 M. Chen and D. W. Goodman, Catalytically active gold: From nanoparticles to ultrathin films, *Acc. Chem. Res.*, 2006, **39**, 739–746.
4 A. S. K. Hashmi, G. J. Hutchings and G. Catalysis, *Angew. Chem., Int. Ed.*, 2006, **45**, 7896–7936.
5 M. Grzelczak, J. Pérez-Juste, P. Mulvaney and L. M. Liz-Marzán, Shape control in gold nanoparticle synthesis, *Chem. Soc. Rev.*, 2008, **37**, 1783–1791.
6 S. Engel, E. C. Fritz and B. J. Ravoo, New trends in the functionalization of metallic gold: From organosulfur ligands to N-heterocyclic carbenes, *Chem. Soc. Rev.*, 2017, **46**, 2057–2075.
7 S. R. Thomas and A. Casini, N-Heterocyclic carbenes as "smart" gold nanoparticle stabilizers: State-of-the art and perspectives for biomedical applications, *J. Organomet. Chem.*, 2021, **938**, 121743.
8 C. Eisen, J. M. Chin and M. R. Reithofer, Catalytically Active Gold Nanomaterials Stabilized by N-heterocyclic Carbenes, *Chem. – Asian J.*, 2021, **16**, 3026–3037.
9 C. A. Smith, M. R. Narouz, P. A. Lummis, I. Singh, A. Nazemi, C.-H. Li and C. M. Crudden, N-Heterocyclic Carbenes in Materials Chemistry, *Chem. Rev.*, 2019, **119**, 4986–5056.
10 H. Shen, G. Tian, Z. Xu, L. Wang, Q. Wu, Y. Zhang, B. K. Teo and N. Zheng, N-heterocyclic carbene coordinated metal nanoparticles and nanoclusters, *Coord. Chem. Rev.*, 2022, **458**, 214425.
11 A. Porcheron, O. Sadek, S. B. Sowid, N. Bridonneau, L. Hippolyte, D. Mercier, P. Marcus, L. Mutalliev, C. Chauvier, C. Chanéac, L. Fensterbank and F. Ribot, Direct Synthesis of Mesoionic Carbene (MIC)-Stabilized Gold Nanoparticles from 1,2,3-Triazolium Salts, *Chem. Mater.*, 2023, **35**, 6865–6876.
12 D. T. H. Nguyen, M. Bélanger-Bouliga, L. R. Shultz, A. Maity, T. Jurca and A. Nazemi, Robust Water-Soluble Gold Nanoparticles via Polymerized Mesoionic N-Heterocyclic Carbene–Gold(I) Complexes, *Chem. Mater.*, 2021, **33**, 9588–9600.
13 L. Cui, M. Du and S. Guo, Preparation, Characterization and Stability Studies of Gold Nanoparticles Capped by 1,2,3-Triazole-Based Mesoionic Carbenes, *ChemistrySelect*, 2022, **7**, e202201999.
14 G. M. D. M. Rúbio, B. K. Keppler, J. M. Chin and M. R. Reithofer, Synthetically Versatile Nitrogen Acyclic Carbene Stabilized Gold Nanoparticles, *Chem. – Eur. J.*, 2020, **26**, 15859–15862.
15 E. C. Hurst, K. Wilson, I. J. S. Fairlamb and V. Chechik, N-Heterocyclic carbene coated metal nanoparticles, *New J. Chem.*, 2009, **33**, 1837–1840.
16 J. Vignolle and T. D. Tilley, N-Heterocyclic carbene-stabilized gold nanoparticles and their assembly into 3D superlattices, *Chem. Commun.*, 2009, **46**, 7230–7232.
17 A. Ferry, K. Schaepe, P. Tegeder, C. Richter, K. M. Chepiga, B. J. Ravoo and F. Glorius, Negatively Charged N-Heterocyclic Carbene-Stabilized Pd and Au Nanoparticles and Efficient Catalysis in Water, *ACS Catal.*, 2015, **5**, 5414–5420.
18 M. J. MacLeod and J. A. Johnson, PEGylated N-Heterocyclic Carbene Anchors Designed to Stabilize Gold Nanoparticles in Biologically Relevant Media, *J. Am. Chem. Soc.*, 2015, **137**, 7974–7977.
19 S. R. Thomas, W. Yang, D. J. Morgan, T. E. Davies, J. J. Li, R. A. Fischer, J. Huang, N. Dimitratos and A. Casini, Bottom-up Synthesis of Water-Soluble Gold Nanoparticles Stabilized by N-Heterocyclic Carbenes: From Structural Characterization to Applications, *Chem. – Eur. J.*, 2022, e202201575.
20 S. G. Song, C. Satheeshkumar, J. Park, J. Ahn, T. Premkumar, Y. Lee and C. Song, N-heterocyclic carbene-based conducting polymer-gold nanoparticle hybrids and their catalytic application, *Macromolecules*, 2014, **47**, 6566–6571.
21 X. X. Gou, T. Liu, Y. Y. Wang and Y. F. Han, Ultrastable and Highly Catalytically Active N-Heterocyclic-Carbene-Stabilized Gold Nanoparticles in Confined Spaces, *Angew. Chem., Int. Ed.*, 2020, **59**, 16683–16689.
22 C. Eisen, L. Ge, E. Santini, J. M. Chin, R. T. Woodward and M. R. Reithofer, Hyper crosslinked polymer supported NHC stabilized gold nanoparticles with excellent catalytic performance in flow processes, *Nanoscale Adv.*, 2023, **5**, 1095–1101.
23 K. Salorinne, R. W. Y. Man, C. H. Li, M. Taki, M. Nambo and C. M. Crudden, Water-Soluble N-Heterocyclic Carbene-Protected Gold Nanoparticles: Size-Controlled Synthesis, Stability, and Optical Properties, *Angew. Chem., Int. Ed.*, 2017, **56**, 6198–6202.

24 M. Bélanger-Bouliga, R. Mahious, P. I. Pitroipa and A. Nazemi, Perylene diimide-taggedN-heterocyclic carbene-stabilized gold nanoparticles: How much ligand desorbs from surface in presence of thiols?, *Dalton Trans.*, 2021, **50**, 5598–5606.

25 C. Eisen, B. K. Keppler, J. M. Chin, X. Su and M. R. Reithofer, Fabrication of azido-PEG-NHC stabilized gold nanoparticles as a functionalizable platform, *Chem. Sci.*, 2024, **15**, 18524–18533.

26 X. Qiao, X. X. Gou, Y. Li, J. L. Li, T. Yue, Q. Sheng and Y. F. Han, Poly(N-heterocyclic carbene)-Protected Water-Soluble Gold Nanoparticles with Tunable Functions for Biosensing Applications, *ACS Appl. Nano Mater.*, 2023, **6**, 2218–2227.

27 A. J. Young, C. Eisen, G. M. D. M. Rubio, J. M. Chin and M. R. Reithofer, pH responsive histidin-2-ylidene stabilized gold nanoparticles, *J. Inorg. Biochem.*, 2019, **199**, 110707.

28 M. Bélanger-Bouliga, N. Kihal, H. Mahious, P. T. Nguyen, S. Bourgault and A. Nazemi, Synthesis and Characterization of Tetraphenylethylene-Functionalized N-Heterocyclic Carbene Stabilized Gold Nanoparticles with Aggregation-Induced Emission, *Can. J. Chem.*, 2023, **101**, 477–486.

29 M. J. MacLeod, A. J. Goodman, H. Z. Ye, H. V. T. Nguyen, T. Van Voorhis and J. A. Johnson, Robust gold nanorods stabilized by bidentate N-heterocyclic-carbene–thiolate ligands, *Nat. Chem.*, 2019, **11**, 57–63.

30 R. W. Y. Man, C. H. Li, M. W. A. MacLean, O. V. Zenkina, M. T. Zamora, L. N. Saunders, A. Rousina-Webb, M. Nambo and C. M. Crudden, Ultrastable gold nanoparticles modified by bidentate N-Heterocyclic Carbene Ligands, *J. Am. Chem. Soc.*, 2018, **140**, 1576–1579.

31 C. J. B. Alejo, C. Fasciani, M. Grenier, J. C. Netto-Ferreira and J. C. Scaiano, Reduction of resazurin to resorufin catalyzed by gold nanoparticles: Dramatic reaction acceleration by laser or LED plasmon excitation, *Catal. Sci. Technol.*, 2011, **1**, 1506–1511.

32 B. Das, J. Lou-Franco, B. Gilbride, M. G. Ellis, L. D. Stewart, I. R. Grant, P. Balasubramanian and C. Cao, Peroxidase-Mimicking Activity of Biogenic Gold Nanoparticles Produced from Prunus nepalensis Fruit Extract: Characterizations and Application for the Detection of Mycobacterium bovis, *ACS Appl. Bio. Mater.*, 2022, **5**, 2712–2725.

33 H. Wei and E. Wang, Nanomaterials with enzyme-like characteristics (nanozymes): Next-generation artificial enzymes, *Chem. Soc. Rev.*, 2013, **42**, 6060–6093.

34 Y. Wu, F. Zeng, Y. Zhao and S. Wu, Emerging contrast agents for multispectral optoacoustic imaging and their biomedical applications, *Chem. Soc. Rev.*, 2021, **50**, 7924–7940.

35 D. Prajapati, C. Schulzke, M. K. Kindermann and A. R. Kapdi, Selective palladium-catalysed arylation of 2,6-dibromopyridine using N-heterocyclic carbene ligands, *RSC Adv.*, 2015, **5**, 53073–53085.

36 G. Papini, M. Pellei, G. G. Lobbia, A. Burini and C. Santini, Sulfonate- or carboxylate-functionalized N-heterocyclic bis-carbene ligands and related water soluble silver complexes, *Dalton Trans.*, 2009, 6985–6990.

37 M. Brust, J. Fink, D. Bethell, D. J. Schiffrin and C. Kiely, Synthesis and Reactions of Functionalised Gold Nanoparticles, *J. Chem. Soc., Chem. Commun.*, 1995, **16**, 1655–1656.

38 C. Guo and J. L. Yarger, Characterizing gold nanoparticles by NMR spectroscopy, *Magn. Reson. Chem.*, 2018, **56**, 1074–1082.

39 A. Leifert, Y. Pan-Bartnek, U. Simon and W. Jahnen-Dechent, Molecularly stabilised ultrasmall gold nanoparticles: Synthesis, characterization and bioactivity, *Nanoscale*, 2013, **5**, 6224–6242.

40 D. J. Pochapski, C. Carvalho dos Santos, G. W. Leite, S. H. Pulcinelli and C. V. Santilli, Zeta Potential and Colloidal Stability Predictions for Inorganic Nanoparticle Dispersions: Effects of Experimental Conditions and Electrokinetic Models on the Interpretation of Results, *Langmuir*, 2021, **37**, 13379–13389.

41 A. Carone, S. Emilsson, P. Mariani, A. Désert and S. Parola, Gold nanoparticle shape dependence of colloidal stability domains, *Nanoscale Adv.*, 2023, **5**, 2017–2026.

42 J. F. Moulder and J. Chastain, *Handbook of X-ray Photoelectron Spectroscopy: A Reference Book of Standard Spectra for Identification and Interpretation of XPS Data, Physical Electronics Division*, Perkin-Elmer Corporation, 1992.

43 N. Fairley, V. Fernandez, M. Richard-Plouet, C. Guillot-Deudon, J. Walton, E. Smith, D. Flahaut, M. Greiner, M. Biesinger, S. Tougaard, D. Morgan and J. Baltrusaitis, Systematic and collaborative approach to problem solving using X-ray photoelectron spectroscopy, *Appl. Surf. Sci. Adv.*, 2021, **5**, 100112.

44 G. Fanali, A. Di Masi, V. Trezza, M. Marino, M. Fasano and P. Ascenzi, Human serum albumin, From bench to bedside, *Mol. Aspects Med.*, 2012, **33**, 209–290.

45 N. Bhatt, P. J. J. Huang, N. Dave and J. Liu, Dissociation and degradation of thiol-modified DNA on gold nanoparticles in aqueous and organic solvents, *Langmuir*, 2011, **27**, 6132–6137.

46 A. Bano, A. Dawood, Rida, F. Saira, A. Malik, M. Alkholief, H. Ahmad, M. A. Khan, Z. Ahmad and O. Bazighifan, Enhancing catalytic activity of gold nanoparticles in a standard redox reaction by investigating the impact of AuNPs size, temperature and reductant concentrations, *Sci. Rep.*, 2023, **13**, 12359.

47 W. Huang, Q. Hua and T. Cao, Influence and removal of capping ligands on catalytic colloidal nanoparticles, *Catal. Lett.*, 2014, 1355–1369.

48 D. Lavogina, H. Lust, M. J. Tahk, T. Laasfeld, H. Vellama, N. Nasirova, M. Vardja, K. L. Eskla, A. Salumets, A. Rinken and J. Jaal, Revisiting the Resazurin–Based Sensing of Cellular Viability, Widening the Application Horizon, *Biosensors*, 2022, **12**, 196.

49 S. A. Sufyan, B. van Devener and M. M. Nigra, Synthesis of Highly Accessible and Reactive Sites in Gold Nanoparticles Using Bound Bis(Diphenylphosphine), Ligands, *Chem. Eur. J.*, 2022, **28**, e202202877.
50 Y. Liu, C. Wang, N. Cai, S. Long and F. Yu, Negatively charged gold nanoparticles as an intrinsic peroxidase mimic and their applications in the oxidation of dopamine, *J. Mater. Sci.*, 2014, **49**, 7143–7150.
51 L. Gao, M. Liu, G. Ma, Y. Wang, L. Zhao, Q. Yuan, F. Gao, R. Liu, J. Zhai, Z. Chai, Y. Zhao and X. Gao, Peptide-Conjugated Gold Nanoprobe: Intrinsic Nanozyme-Linked Immunsorbant Assay of Integrin Expression Level on Cell Membrane, *ACS Nano*, 2015, **9**, 10979–10990.
52 Z. Huang, B. Liu and J. Liu, Enhancing the peroxidase-like activity and stability of gold nanoparticles by coating a partial iron phosphate shell, *Nanoscale*, 2020, **12**, 22467–22472.
53 Y. Jv, B. Li and R. Cao, Positively-charged gold nanoparticles as peroxidiase mimic and their application in hydrogen peroxide and glucose detection, *Chem. Commun.*, 2010, **46**, 8017–8019.
54 P. Tegeder, M. Freitag, K. M. Chepiga, S. Muratsugu, N. Möller, S. Lamping, M. Tada, F. Glorius and B. J. Ravoo, N-Heterocyclic Carbene-Modified Au–Pd Alloy Nanoparticles and Their Application as Biomimetic and Heterogeneous Catalysts, *Chem. – Eur. J.*, 2018, **24**, 18682–18688.
55 G. R. Lopes, D. C. G. A. Pinto and A. M. S. Silva, Horseradish peroxidase (HRP) as a tool in green chemistry, *RSC Adv.*, 2014, **4**, 37244–37265.
56 P. D. Josephy, T. Eling and R. P. Mason, The horseradish peroxidase-catalyzed oxidation of 3,5,3′,5′-tetramethylbenzidine. Free radical and charge-transfer complex intermediates., *J. Biol. Chem.*, 1982, **257**, 3669–3675.
57 J. Liu, D. Yang, W. Hu, N. Huang, Y. Rong, Y. Long and H. Zheng, Piezoelectric BaTiO3 nanoparticles as oxidase mimics breaking pH limitation for colorimetric detection of glutathione reductase, *Chem. Eng. J.*, 2024, 481, DOI: 10.1016/j.cej.2024.148609.
58 B. Liu and J. Liu, Accelerating peroxidase mimicking nanozymes using DNA, *Nanoscale*, 2015, **7**, 13831–13835.
59 S. Nuti, J. Fernández-Lodeiro, J. M. Palomo, J. L. Capelo-Martinez, C. Lodeiro and A. Fernández-Lodeiro, Synthesis, Structural Analysis, and Peroxidase-Mimicking Activity of AuPt Branched Nanoparticles, *Nanomaterials*, 2024, **14**, 1166.
60 V. T. C. Tsang, X. Li and T. T. W. Wong, A review of endogenous and exogenous contrast agents used in photoacoustic tomography with different sensing configurations, *Sensors*, 2020, **20**, 5595.
61 W. Li and X. Chen, Gold nanoparticles for photoacoustic imaging, *Nanomedicine*, 2015, **10**, 299–320.
62 A. Taruttis and V. Ntziachristos, Advances in real-time multispectral optoacoustic imaging and its applications, *Nat. Photonics*, 2015, **9**, 219–227.
63 A. Kavalaraki, E. Spyratou, M. A. Kouri and E. P. Efstathopoulos, Gold Nanoparticles as Contrast Agents in Ophthalmic Imaging, *Optics*, 2023, **4**, 74–99.
64 P. Huang, J. Lin, W. Li, P. Rong, Z. Wang, S. Wang, X. Wang, X. Sun, M. Aronova, G. Niu, R. D. Leapman, Z. Nie and X. Chen, Biodegradable gold nanovesicles with an ultrastrong plasmonic coupling effect for photoacoustic imaging and photothermal therapy, *Angew. Chem., Int. Ed.*, 2013, **52**, 13958–13964.
65 Y. Mantri and J. V. Jokerst, Engineering Plasmonic Nanoparticles for Enhanced Photoacoustic Imaging, *ACS Nano*, 2020, **14**, 9408–9422.
66 V. P. Nguyen, Y. Li, J. Henry, W. Zhang, X. Wang and Y. M. Paulus, Gold Nanorod Enhanced Photoacoustic Microscopy and Optical Coherence Tomography of Choroidal Neovascularization, *ACS Appl. Mater. Interfaces*, 2021, **13**, 40214–40228.
67 P. Huang, J. Lin, W. Li, P. Rong, Z. Wang, S. Wang, X. Wang, X. Sun, M. Aronova, G. Niu, R. D. Leapman, Z. Nie and X. Chen, Biodegradable gold nanovesicles with an ultrastrong plasmonic coupling effect for photoacoustic imaging and photothermal therapy, *Angew. Chem., Int. Ed.*, 2013, **52**, 13958–13964.